Research article

Kevin T. Crampton, Alan G. Joly and Patrick Z. El-Khoury*

Surface plasmon polariton pulse shaping via two-dimensional Bragg grating pairs

https://doi.org/10.1515/nanoph-2020-0522
Received September 11, 2020; accepted October 25, 2020;
published online November 9, 2020

Abstract: We demonstrate control over the spatial and temporal properties of surface plasmon polaritons (SPPs) launched from nanohole arrays in silver. The arrays provide wave vector matching to allow the conversion of free-space photons into counter-propagating SPPs. SPPs launched from multiple arrays interfere at well-defined spatial positions, and the interference fringes form an all-SPP periodic nano-optical grating which evolves in space and time as the SPPs propagate. The spatio-temporal characteristics of the optical grating can be tuned through various nanohole array parameters such as tilt angle, separation, and array width. In addition, we examine multiperiodic arrays (MPAs) consisting of arrays with different pitches placed adjacent to one another. This platform allows the temporal interference of SPPs with different central wavelengths to be tailored through the MPA geometric and structural parameters. The temporal interference serves as an encoded signal, whereby the frequency components can be controlled by the array properties.

Keywords: nanohole array; PEEM; photonic Bragg grating; plasmon interference; pulse shaping; surface plasmon polariton.

Surface plasmon polaritons (SPPs) are electron charge-density waves that may be excited at the boundary between metals and dielectrics. Due to their interfacial confinement, the integration of SPPs in photonic devices is anticipated to bridge the gap between the microlength and nanolength scales in optical circuit development, effectively miniaturizing and boosting the information transfer rates of traditional electronic circuitry [1–3]. This requires intricate knowledge of the optical properties of SPPs and control over their electromagnetic interactions. Research into the development of interfacial plasmonic optics aimed at controlling the (out)coupling [4–9], direction [10–14], and focusing [15–20] of SPP fields has been motivated by these objectives. One common feature of such systems is that they utilize micro- or nanopatterned plasmonic components to achieve coupling. This generally leads to SPP fields that closely mimic the temporal properties of the excitation fields. To reach the next level of design, detailed control of the SPP fields themselves is desirable. Both the spatial and spectral characteristics are relevant design parameters in this context.

For metallic substrates, SPPs arise as a result of coupling between coherent oscillations of the surface electrons and external fields, as described by the planar metal dispersion. Periodic systems, by comparison, sustain Bloch-wave SPPs that may be excited at the stop-band frequency of polaritonic crystals [21–23]. In such systems, the crystal structure governs the electromagnetic fields that may be sustained at its interface, offering multiple degrees of freedom for structuring the spatial and spectral distributions of SPP fields. In addition, under the right conditions, these interfaces can support negative refractory effects as evidenced by recent reports [12, 21, 24, 25]. While still relying on the linear interactions between SPPs, multielement plasmonic devices that exploit the sensitivity of periodic coupling structures are poised to enable the spatial and spectral manipulation of SPP fields. This lays the framework for advanced varieties of two-dimensional (2D) ultrafast plasmonic communication and computing platforms, as described in a recent review article [2].

In this work, we utilize pairs of 2D photonic Bragg gratings (2PGs) etched in silver to explore different ways to utilize SPP fields as photonic elements, either through spatial or temporal (frequency) modulation. Our experimental methods are based on 2PG pairs composed of square arrays of nanoholes, which couple light into counter-propagating SPPs. We explore two unique configurations

***Corresponding author: Patrick Z. El-Khoury**, Physical Sciences Division, Pacific Northwest National Laboratory, P.O. Box 999, Richland, Washington 99352, USA, E-mail: patrick.elkhoury@pnnl.gov. https://orcid.org/0000-0002-6032-9006
Kevin T. Crampton and Alan G. Joly, Physical Sciences Division, Pacific Northwest National Laboratory, P.O. Box 999, Richland, Washington 99352, USA. https://orcid.org/0000-0002-1258-7895 (K.T. Crampton). https://orcid.org/0000-0003-2931-4524 (A.G. Joly)

aimed at controlling and visualizing spatial and temporal SPP evolution: (1) SPP-based spatial grating generation, and (2) SPP carrier-wave modulation. The first configuration involves spatially offset, rotated 2PG pairs that are utilized to generate SPP-derived spatial gratings, which we image in real space through time-resolved photoemission electron microscopy (PEEM) [26–28]. PEEM is a robust tool for surface microscopy that has been widely employed to study both localized [28–31] and propagating SPPs [6, 30, 32–35]. Our present design employs noncollinear SPPs which propagate and interfere over a volume governed by the 2PG geometric parameters, periodicity, and orientation. This allows the spatial intensity patterns of SPP fields to be tailored in amplitude and phase. In our second approach, a multi-periodic 2PG is utilized to manipulate the SPP field carrier wave amplitude through the temporal interference of multi-color plasmons. In effect, we realize a 2D amplitude modulator or synthesizer, now operating at optical frequencies. These complementary approaches may be regarded as spatial and temporal analogs of tailored SPP interference.

1 Methods and results

The 2PGs we employ comprised square arrays of nanoholes that are fabricated using focused-ion beam milling of a 100 nm thick, sputtered silver film over mica. The hole depth and diameter are fixed at 100 nm which fully exposes the underlying mica substrate within the holes. The hole spacing or pitch (Λ) is reserved as an experimental parameter that may be tuned to satisfy the momentum-matching requirement for SPP excitation. Experimentally, we use the two-color interferometric time-resolved PEEM (ITR-PEEM) approach which maps SPP evolution through 2-photon photoemission (2PPE) [27, 28]. In our present implementation, SPP fields are excited and interrogated using up to three separate pulses, comprised of a red pulse pair centered at λ = 780 ($\delta\lambda$ = 55 nm FWHM, 20 fs) and an additional blue pulse at λ = 390 ($\delta\lambda$ = 8 nm, 60 fs) nm. The latter is derived from the red pulses via second-harmonic generation. The silver work function dictates that three red photons are required to achieve photoemission in a third-order process. Using a blue second harmonic photon in place of two red photons lowers the order to quadratic and increases the signal level.

A schematic description of the experiment is shown in Figure 1a. Separate phase-locked red pulses are used to launch SPPs from each array. This is accomplished by splitting the pump field in a Michelson interferometer, which is also utilized to actively stabilize the relative phase between the two red laser fields in real time during the measurement. Tuning the 2PG pitch, Λ, allows momentum matching in the backward (-x, counter-propagating) direction according to the condition $-k_{\mathrm{spp}} = k_l' - 2\pi/\Lambda$, where $k_l' = k_l \sin\varphi$ is the in-plane laser excitation wave vector, φ is the excitation angle measured from the surface normal, and k_{spp} is determined from the silver dielectric and excitation wavelength. For our conditions, the linear dispersion of silver, pump center wavelength of 780 nm, and angle of incidence of 75° establish that lattice spacing of ~400 nm excites counter-propagating SPPs (see Figure 2a), which we focus on exclusively in this work. Once excited, the counter-propagating SPP wave packets travel with group velocity previously measured as ~0.95c [34, 35] in thin silver. The time-delayed blue pulse then interrogates the surface field leading to photoemission. The spot size of the blue pulse is adjusted such that it encompasses nearly the entire field-of-view. By tuning the time delay of the blue pulse, the SPP surface field is mapped at different spatial positions from the arrays. This is shown in Figure 1b,c which display PEEM images acquired using blue time delays of 267 and 350 fs corresponding to spatial offsets of 80 and 105 μm from the generating arrays. The tilt applied to the 2PG of $\theta = \pm 5°$ allows the SPPs to intersect at a well-defined point. The resulting SPP superposition is marked by lateral oscillations that evolve as the time delay is increased. This is clearer in the full SPP surface maps we present in Figure 2b. The 2PPE image is time-integrated. In other works, this image was generated by averaging images taken at different blue pulse time delays. Periodic lateral oscillations in the field arise near the SPP convergence point and persist for the duration of the trajectory (Figure 2b). Unlike a linear superposition of degenerate plane waves, which would sustain a fixed-period grating at all points of envelope overlap, the SPP-derived fringe spacing changes in space as the individual fields evolve. Figure 2c displays a finite-difference time-domain (FDTD) calculation which closely mimics our experimental configuration. The FDTD results reproduce the evolving fringe spacing nearly perfectly. The exact nature of the fringe evolution is dependent on the spacing between arrays, array angle, and array width and is reminiscent of the interference of apertured fields, analogous to Young's double slit experiment with the arrays themselves acting as finite apertures (slits). As a result of SPP interference, we have a tunable grating spacing that can be changed with distance, array spacing (aperture spacing) and array lateral dimensions.

In accordance with the grating coupling condition, the lateral separation between the arrays, their angles relative to the plane of incidence (see Figure 1), the pump central

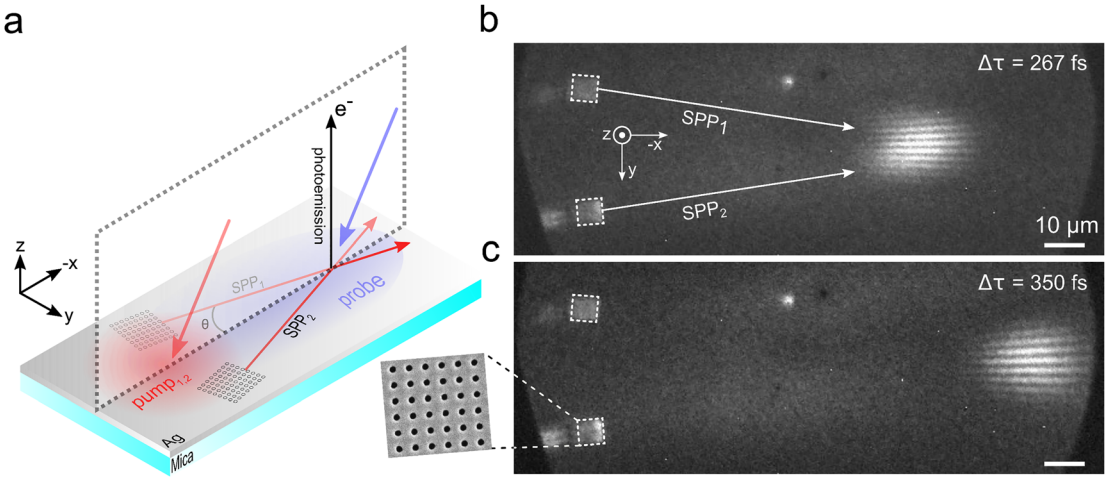

Figure 1: Tunable surface plasmon polariton (SPP) spatial grating creation via angled 2D photonic Bragg gratings (2PGs). (a) Experimental configuration for photoemission electron microscopy (PEEM) imaging of spatial gratings. The 2PGs are composed of 400 nm pitch square arrays of nanoholes oriented at $\theta = \pm 5°$ relative to the plane of incidence (dashed square). A phase-locked 780 nm pulse pair is directed such that each array is excited by a single pulse. The resulting SPPs travel counter to the incident laser fields and interfere spatially and temporally at a controllable point. The SPP surface field is readout by a 390 nm pulse that encompasses the excitation and interference areas. As the delay between the pump fields and blue readout pulse is varied, the PEEM image captures the evolution of the SPP fields at different spatial points as shown in (b) for a blue delay 267 fs, and (c) a blue delay 350 fs. The positions of the 2PG pairs are indicated by the dashed boxes in b and c. A scanning electron micrograph of a single 2PG is shown in c.

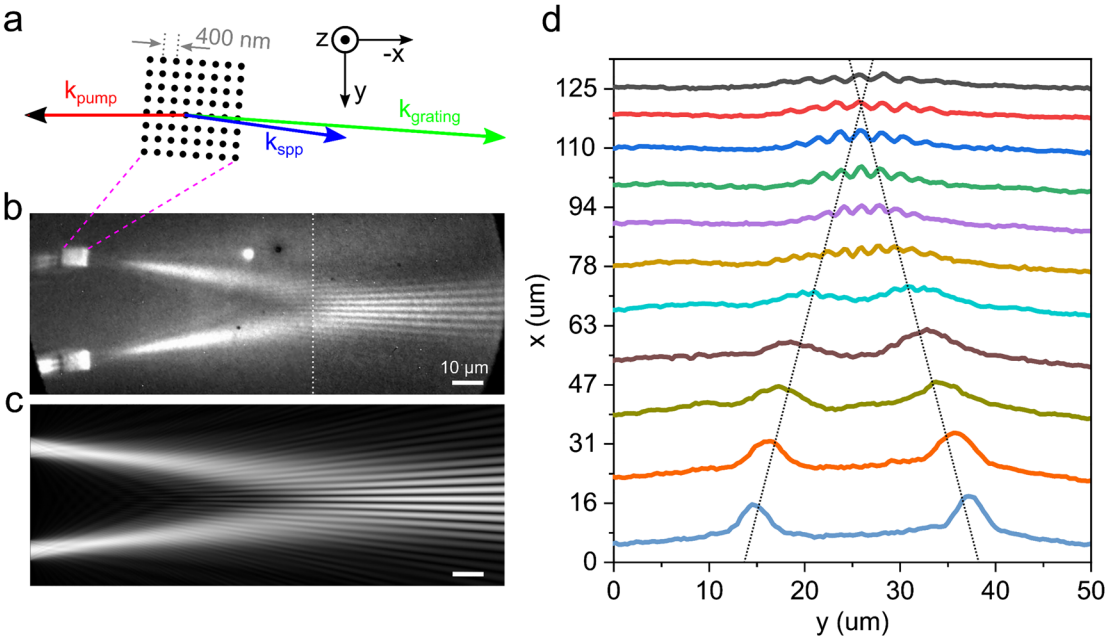

Figure 2: (a) Wave vector matching diagram for counter-propagating surface plasmon polariton (SPP) excitation at an angle superposed on a schematic of the 2D photonic Bragg grating (2PG). (b) Time-integrated 2-photon photoemission (2PPE) image of SPP surface fields displaying spatial interference. Note, the image contrast was enhanced on the right-hand side of the dashed line. The periodic intensity modulation evolves as the SPPs propagate, as evidenced by the change in fringe spacing. (c) The profile may be recovered by explicitly describing the diverging plasmonic fields and their time evolution through finite-difference time-domain (FDTD) simulations. (d) Profiles extracted from the image measured in b. The trajectories of the nascent SPP are indicated by the dashed lines.

wavelength, and the silver dielectric constants together dictate the SPP intersection point. As depicted by the wave vector matching diagram shown in Figure 2a, 2PG tilts of $\theta = \pm 5°$ and a lateral separation of 25 μm position the SPP intersection point at ~80 μm from the arrays. Thus, the exact position of the intersection can be carefully controlled simply by tuning the array parameters, as we have shown elsewhere using a single 2PG steering element [14]. 2PG angles of ±4–6° allow both the SPP intersection points and interference patterns to be visualized within the decay length and our 150 μm field-of-view. In the array pair depicted in Figure 2, the grating spacing varies from about 1.8 μm to over 2.5 μm over the interference region shown. Due to the fact that the evolution of the fringe spacing depends on the array pair parameters, the 2PG geometry may be tailored to generate SPP that more closely mimic plane-waves. This would produce interference patterns, where the grating spacing is less divergent with evolution. The length over which the grating can be sustained is governed by both the SPP coherence length and absorptive losses in the metal, both of which serve to lessen the interference intensity. Using ITR-PEEM, we have previously measured SPPs at distances over 250 microns from the source [6]. At larger angles, the decay in grating fringes is determined by the field overlap length while at very small angles, the nearly collinear beams dictate that SPP coherence and/or intensity decay may be the limiting factor.

The ability to control the spatial and temporal evolution of SPP fields opens up several avenues for tailoring optical signals in the near-field. For instance, the grating in Figure 2b can be used to diffract a variably delayed SPP field into a well-defined direction, analogous to an optical four-wave mixing experiment or transient grating. SPPs launched with different angles or central wavelengths can diffract to different spatial regions depending on where they interact with the SPP grating. In addition, the ability to tune the SPP central wavelength allows other possibilities for information encoding through field amplitude modulation. A simple extension of the results from Figure 2 demonstrate the power of this approach, which we expand on below.

We have previously shown that the nanohole array acts as a filter for the incoming field, resulting in counter-propagating SPPs that can have spectra that are frequency shifted from the excitation laser spectrum [36]. This occurs because the counter-propagating surface plasmon sustained by the array may be narrower and/or shifted from the input (red) pulse spectrum (~55 nm FWHM). As a result, only a portion of the input bandwidth is efficiently converted into the SPP. A simple way to tune the array resonance is to change the pitch. This necessitates that a different region of the input pulse spectrum will couple to generate the counter-propagating SPP. As we have previously shown, an array with pitch of 380 nm will generate an SPP with a substantially different frequency spectrum relative to using an array with pitch of 400 nm or above [36].

We exploit this concept by fabricating multiperiodic arrays (MPA) comprised of adjacent 2PGs of different pitches, namely Λ = 430 and 370 nm. A schematic of a multiperiodic 2PG is shown in Figure 3a. In comparison to the previous example, in this case the slight difference in wave vector leads to spatial interference fringes that move laterally with the difference wave vector spatial frequency and thereby depend on propagation distance from the array. We employ methods similar to the spatial grating experiments described above for sample fabrication. We interrogate the frequency components of the MPA-derived plasmons through interferometric autocorrelation [36, 37], where the delay between two red phase-locked pulses is varied and photoemission is facilitated through interaction with the blue pulse. We introduce a time delay between the 390 nm blue pulse and the first red pulse to position the reference SPP 70 μm from the array. A 2PPE image of the MPA and reference SPP is shown in Figure 3b. Given that the individual 2PGs that comprise the MPA are milled adjacent to one another, the counter-propagating plasmons are laterally separated but overlapping; their profiles are indicated by the ovals in Figure 3b. To acquire the autocorrelation trace, the second red pulse is interferometrically scanned in time relative to the first while keeping the reference SPP/blue pulse time (space) coincident. Autocorrelation traces are acquired through 2PPE by spatially integrating the reference SPP profile (see Figure 3b) at every time delay as the test SPP sweeps over it in space. Centering the integration window on the MPA itself recovers the second-order interferometric autocorrelation of the pump pulses (Figure 3c, upper pane). When centered on the reference SPP, the autocorrelation is first order and modulations appear in the wings of the envelope (Figure 3c, lower pane). The amplitude modulation establishes that the 430 and 370 nm 2PG sustain SPPs of unique wavelengths which then interfere along the propagation pathway. We retrieve their spectra through discrete Fourier transformation of the autocorrelation. The results are summarized in Figure 4. The recovered spectrum (Figure 4b, black curve) fits well to the sum of constitutive Gaussian SPP spectra. The parameters of the 370 nm-generated SPP (λ = 775, $\delta\lambda$ = 45 nm) are marginally different than the pulse parameters (λ = 780 nm, $\delta\lambda$ = 55 nm), while the longer wavelength mode is significantly red-shifted

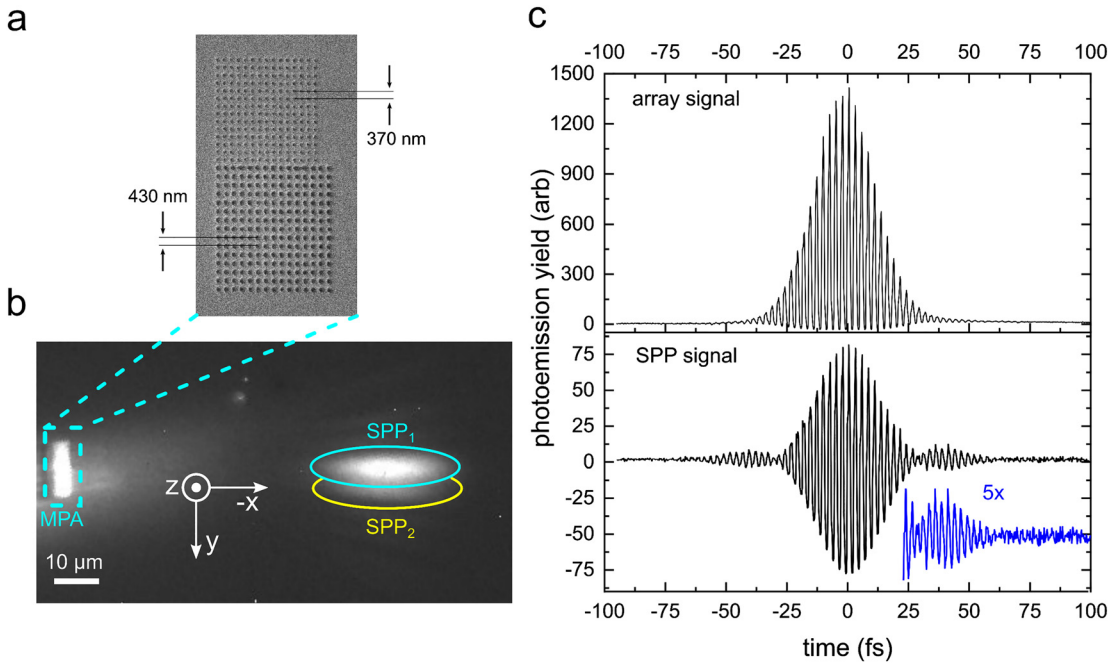

Figure 3: Amplitude modulation of an surface plasmon polariton (SPP) wave packet.
(a) Scanning electron micrograph of a multiperiodic array composed of adjacent 2D photonic Bragg gratings (2PG) of different pitches. b) Two-photon photoemission (2PPE) snapshot of reference SPP after 70 μm of propagation. The orientation of the multiperiodic array (MPA) (dashed box) is as pictured in a. (c) Interferometric autocorrelation traces for signal originating at the array and signal derived from SPP overlap 70 microns from the array.

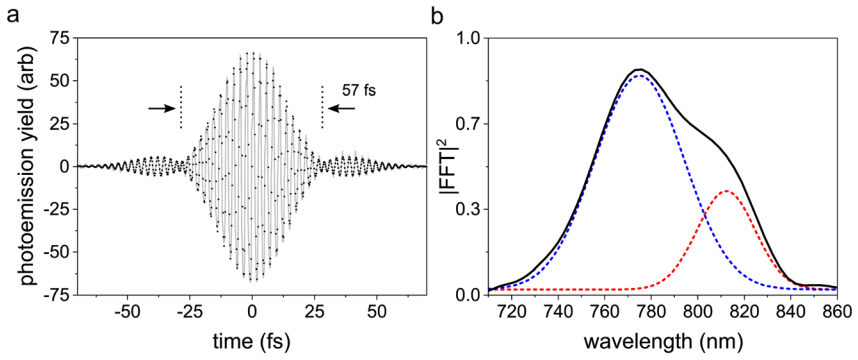

Figure 4: Time and frequency analysis of the multiperiodic array (MPA)-derived wave packet.
(a) Autocorrelation trace presented in Figure 3c fitted to an analytical model of the total fields. (b) Frequency domain representation of the time profile.

and narrowed (λ = 815 nm, $\delta\lambda$ = 35 nm). The energy detuning of 72 meV agrees with the modulation period of 57 fs, as highlighted in Figure 4a. An analytical model for the SPP fields that utilizes the parameters extracted from the frequency-domain fit reproduces the observed time profile with high fidelity (black dots superimposed on experimental trace shown in gray, Figure 4a).

The information encoded in the MPA-derived wave packet now consists of the original SPP frequencies, their amplitudes, and a slowly varying modulation that arises at the beat frequency between the waves. The result is a Fourier pair that can be tailored by utilizing 2PGs with different pitches. Multiple MPAs can therefore provide a convenient way to transmit modulated signals or may be used as elements for pulse shaping.

2 Conclusions

We have demonstrated that control over the SPP spatial and temporal (spectral) properties can be achieved via interference between carefully chosen counter-propagating SPPs. Two such SPPs interacting at an angle produce a spatial interference pattern (grating)

that changes in space as the two SPPs evolve. The position and fringe spacing can be controlled through array parameters such as angle, separation, and width, reminiscent of apertured field interference. A simple extension to the spatial grating technique involves placing two arrays with different pitches next to one another. Such an MPA system produces SPPs with temporal modulation determined by the interference of the coupled SPPs. This allows for simple pulse shaping as well as amplitude modulation of the SPP signals that can be controlled by array properties.

Although carried out in thin silver using prototypical nanohole arrays, it is important to emphasize that our pulse shaping modalities are generally applicable. Utilizing high-index dielectric or semiconductor-based media in combination with pure metals would allow the SPP dispersion to be tuned, in effect, adding another level of control over the spatial and temporal properties of the surface fields(s) [38–40]. Varying the substrate composition also has the advantage of extending the spectral range over which SPPs and analogous matter waves may be sustained. Such an integrated photonic device was explored recently using atomically thin Van der Waals crystals [38]. Another interesting avenue that recognizes the demand for actively controlled polaritonic devices would be to integrate gate-tunable materials, such as graphene, with the electromagnetic field modulation we achieved through SPP spatial interference. As shown recently using hybrid phonon-polariton modes [41], this would allow active control over the SPP spatial interference, similar to what has already been achieved using graphene plasmons [42–44].

Acknowledgement: The authors acknowledge support from the US Department of Energy (DOE), Office of Science, Office of Basic Energy Sciences, Division of Chemical Sciences, Geosciences & Biosciences. This work was performed in EMSL, a national scientific user facility sponsored by DOE's Office of Biological and Environmental Research and located at PNNL. PNNL is operated by Battelle Memorial Institute for the United States Department of Energy.

Author contribution: All the authors have accepted responsibility for the entire content of this submitted manuscript and approved submission.

Research funding: The authors acknowledge support from the US Department of Energy (DOE), Office of Science, Office of Basic Energy Sciences, Division of Chemical Sciences, Geosciences & Biosciences.

Conflict of interest statement: The authors declare no conflicts of interest regarding this article.

References

[1] M. L. Brongersma, R. Zia, and J. A. Schuller, "Plasmonics – the missing link between nanoelectronics and microphotonics," *Appl. Phys. A*, vol. 89, p. 221, 2007.

[2] T. J. Davis, D. E. Gómez, and A. Roberts, "Plasmonic circuits for manipulating optical information," *Nanophotonics*, vol. 6, p. 543, 2016.

[3] W. L. Barnes, A. Dereux, and T. W. Ebbesen, "Surface plasmon subwavelength optics," *Nature*, vol. 424, p. 824, 2003.

[4] E. Devaux, T. W. Ebbesen, J.-C. Weeber, and A. Dereux, "Launching and decoupling surface plasmons via micro-gratings," *Appl. Phys. Lett.*, vol. 83, p. 4936, 2003.

[5] F. López-Tejeira, S. G. Rodrigo, L. Martín-Moreno, et al., "Efficient unidirectional nanoslit couplers for surface plasmons," *Nat. Phys.*, vol. 3, p. 324, 2007.

[6] Y. Gong, A. G. Joly, D. Hu, P. Z. El-Khoury, and W. P. Hess, "Ultrafast imaging of surface plasmons propagating on a gold surface," *Nano Lett.*, vol. 15, p. 3472, 2015.

[7] L. Zhang, A. Kubo, L. Wang, H. Petek, and T. Seideman, "Imaging of surface plasmon polariton fields excited at a nanometer-scale slit," *Phys. Rev. B*, vol. 84, p. 245442, 2011.

[8] B. Hecht, H. Bielefeldt, L. Novotny, Y. Inouye, and D. W. Pohl, "Local excitation, scattering, and interference of surface plasmons," *Phys. Rev. Lett.*, vol. 77, p. 1889, 1996.

[9] Z. Hirboodvash, M. Khodami, N. R. Fong, et al., "Grating couplers fabricated by e-beam lithography for long-range surface plasmon waveguides embedded in a fluoropolymer," *Appl. Opt.*, vol. 58, p. 2994, 2019.

[10] I. Epstein and A. Arie, "Arbitrary bending plasmonic light waves," *Phys. Rev. Lett.*, vol. 112, p. 023903, 2014.

[11] A. Drezet, A. Hohenau, A. L. Stepanov, et al., "Surface plasmon polariton mach–zehnder interferometer and oscillation fringes," *Plasmonics*, vol. 1, p. 141, 2006.

[12] M. U. González, J. C. Weeber, A. L. Baudrion, et al., "Design, near-field characterization, and modeling of 45° surface-plasmon Bragg mirrors," *Phys. Rev. B*, vol. 73, p. 155416, 2006.

[13] V. Pacheco-Peña and M. Beruete, "Steering surface plasmons with a graded index dielectric medium," *J. Phys. D Appl.* Phys., vol. 51, p. 485101, 2018.

[14] K. T. Crampton, A. G. Joly, and P. El-Khoury, "Femtosecond photoemission electron microscopy of surface plasmon polariton beam steering via nanohole arrays," *J. Chem. Phys.*, vol. 153, p. 081103, 2020.

[15] Y. Gong, A. G. Joly, P. Z. El-Khoury, and W. P. Hess, "Interferometric plasmonic lensing with nanohole arrays," *J. Phys. Chem. Lett.*, vol. 5, p. 4243, 2014.

[16] X. Fan and G. P. Wang, "Nanoscale metal waveguide arrays as plasmon lenses," *Opt. Lett.*, vol. 31, p. 1322, 2006.

[17] L. Feng, K. A. Tetz, B. Slutsky, V. Lomakin, and Y. Fainman, "Fourier plasmonics: diffractive focusing of in-plane surface plasmon polariton waves," *Appl. Phys. Lett.*, vol. 91, p. 081101, 2007.

[18] I. P. Radko, S. I. Bozhevolnyi, A. B. Evlyukhin, and A. Boltasseva, "Surface plasmon polariton beam focusing with parabolic nanoparticle chains," *Opt. Exp.*, vol. 15, p. 6576, 2007.

[19] Z. Liu, J. M. Steele, W. Srituravanich, Y. Pikus, C. Sun, and X. Zhang, "Focusing surface plasmons with a plasmonic lens," *Nano Lett.*, vol. 5, p. 1726, 2005.

[20] T. Tanemura, K. C. Balram, D. S. Ly-Gagnon, et al., "Multiple-wavelength focusing of surface plasmons with a nonperiodic nanoslit coupler," *Nano Lett.*, vol. 11, p. 2693, 2011.
[21] S.-H. Chang, S. K. Gray, and G. C. Schatz, "Surface plasmon generation and light transmission by isolated nanoholes and arrays of nanoholes in thin metal films," *Opt. Exp.*, vol. 13, p. 3150, 2005.
[22] S. C. Kitson, W. L. Barnes, and J. R. Sambles, "Full photonic band gap for surface modes in the visible," *Phys. Rev. Lett.*, vol. 77, p. 2670, 1996.
[23] Z. Chen, I. R. Hooper, and J. R. Sambles, "Photonic bandgaps for grating-coupled waveguide modes with a silver tunnel barrier," *New J. Phys.*, vol. 9, p. 251, 2007.
[24] B. Stein, J. Y. Laluet, E. Devaux, C. Genet, and T. W. Ebbesen, "Surface plasmon mode steering and negative refraction," *Phys. Rev. Lett.*, vol. 105, p. 266804, 2010.
[25] C. Luo, S. G. Johnson, J. Joannopoulos, and J. Pendry, "Negative refraction without negative index in metallic photonic crystals," *Opt. Exp.*, vol. 11, p. 746, 2003.
[26] M. Dąbrowski, Y. Dai, and H. Petek, "Ultrafast photoemission electron microscopy: imaging plasmons in space and time," *Chem. Rev.*, 2020.
[27] O. Schmidt, M. Bauer, C. Wiemann, et al., "Time-resolved two photon photoemission electron microscopy," *Appl. Phy. B*, vol. 74, p. 223, 2002.
[28] A. Kubo, K. Onda, H. Petek, Z. Sun, Y. S. Jung, and H. K. Kim, "Femtosecond imaging of surface plasmon dynamics in a nanostructured silver film," *Nano Lett.*, vol. 5, p. 1123, 2005.
[29] Q. Sun, K. Ueno, H. Yu, A. Kubo, Y. Matsuo, and H. Misawa, "Direct imaging of the near field and dynamics of surface plasmon resonance on gold nanostructures using photoemission electron microscopy," *Light Sci. Appl.*, vol. 2, p. e118, 2013.
[30] F. J. Meyer zu Heringdorf, L. I. Chelaru, S. Möllenbeck, D. Thien, and M. Horn-von Hoegen, "Femtosecond photoemission microscopy," *Surf. Sci.*, vol. 601, p. 4700, 2007.
[31] M. Cinchetti, A. Gloskovskii, S. Nepjiko, G. Schönhense, H. Rochholz, and M. Kreiter, "Photoemission electron microscopy as a tool for the investigation of optical near fields," *Phys. Rev. Lett.*, vol. 95, p. 047601, 2005.
[32] A. Kubo, N. Pontius, and H. Petek, "Femtosecond microscopy of surface plasmon polariton wave packet evolution at the silver/vacuum interface," *Nano Lett.*, vol. 7, p. 470, 2007.
[33] P. Kahl, S. Wall, C. Witt, et al., "Normal-incidence photoemission electron microscopy (NI-PEEM) for imaging surface plasmon polaritons," *Plasmonics*, vol. 9, p. 1401, 2014.
[34] C. Lemke, T. Leißner, S. Jauernik, et al., "Mapping surface plasmon polariton propagation via counter-propagating light pulses," *Opt. Exp.*, vol. 20, p. 12877, 2012.
[35] K. T. Crampton, A. G. Joly, and P. Z. El-Khoury, "Direct visualization of counter-propagating surface plasmons in real space-time," *J. Phys. Chem. Lett.*, p. 5694, 2019, https://doi.org/10.1021/acs.jpclett.9b02151.
[36] K. T. Crampton, A. G. Joly, and P. Z. El-Khoury, "Interferometric imaging and spectroscopy of spatio-spectrally tailored surface plasmon polaritons," unpublished, 2020.
[37] C. Lemke, T. Leißner, A. Klick, et al., "Measurement of surface plasmon autocorrelation functions," *Opt. Exp.*, vol. 21, p. 27392, 2013.
[38] H. Zhang, B. Abhiraman, Q. Zhang, et al., "Hybrid exciton-plasmon-polaritons in van der Waals semiconductor gratings," *Nat. Commun.*, vol. 11, p. 3552, 2020.
[39] M. Pelc, W. Jaskólski, A. Ayuela, and L. Chico, "Topologically confined states at corrugations of gated bilayer graphene," *Phys. Rev. B*, vol. 92, p. 085433, 2015.
[40] Q. Wang, X. Yuan, P. Tan, and D. Zhang, "Phase modulation of surface plasmon polaritons by surface relief dielectric structures," *Opt. Exp.*, vol. 16, p. 19271, 2008.
[41] Q. Zhang, Z. Zhen, C. Liu, D. Jariwala, and X. Cui, "Gate-tunable polariton superlens in 2D/3D heterostructures," *Opt. Exp.*, vol. 27, p. 18628, 2019.
[42] J. Chen, M. Badioli, P. Alonso-González, et al., "Optical nano-imaging of gate-tunable graphene plasmons," *Nature*, vol. 487, p. 77, 2012.
[43] G. X. Ni, L. Wang, M. D. Goldflam, et al., "Ultrafast optical switching of infrared plasmon polaritons in high-mobility graphene," *Nat. Photonics*, vol. 10, p. 244, 2016.
[44] B. Yao, Y. Liu, S.-W. Huang, et al., "Broadband gate-tunable terahertz plasmons in graphene heterostructures," *Nat. Photonics*, vol. 12, p. 22, 2018.